Summer Deep Depressions Increase Over the Eastern North Atlantic

Fabio d'Andrea, Jean-Philippe Duvel, Gwendal Rivière, Robert Vautard, Christophe Cassou, Julien Cattiaux, Dim Coumou, Davide Faranda, Tamara Happé, Aglaé Jézéquel, et al.

Geophysical Research Letters

RESEARCH LETTER
10.1029/2023GL104435

Summer Deep Depressions Increase Over the Eastern North Atlantic

Fabio D'Andrea[1], Jean-Philippe Duvel[1], Gwendal Rivière[1], Robert Vautard[2], Christophe Cassou[1,3], Julien Cattiaux[4], Dim Coumou[2,5,6], Davide Faranda[1,7], Tamara Happé[5], Aglaé Jézéquel[1,8], Aurelien Ribes[4], and Pascal Yiou[7]

[1]Laboratoire de Météorologie Dynamique - IPSL, ENS, PSL Research University, École Polytechnique, Institut Polytechnique de Paris, Sorbonne Université, CNRS, Paris, France, [2]Institut Pierre-Simon Laplace, CNRS, Université Paris-Saclay, Sorbonne Université, Paris, France, [3]Centre Européen de Recherche et de Formation Avancée en Calcul Scientifique, CNRS, UMR 5318, Toulouse, France, [4]CNRM, Université de Toulouse, Météo-France, CNRS, Toulouse, France, [5]Institute for Environmental Studies, Vrije Universiteit Amsterdam, Amsterdam, The Netherlands, [6]Royal Netherlands Meteorological Institute (KNMI), De Bilt, The Netherlands, [7]Laboratoire des Sciences du Climat et de l'Environnement, UMR 8212 CEA-CNRS-UVSQ, Université Paris-Saclay and IPSL, Gif-sur-Yvette, France, [8]Ecole des Ponts, Marne-la-Vallée, France

Abstract Mid-tropospheric deep depressions in summer over the North Atlantic are shown to have strongly increased in the eastern and strongly decreased in the western North Atlantic region. This evolution is linked to a change in baroclinicity in the west of the North Atlantic ocean and over the North American coast, likely due to the increased surface temperature there. Deep depressions in the Eastern North Atlantic are linked to a temperature pattern typical of extreme heat events in the region. The same analysis is applied to a sample of CMIP6 model outputs, and no such trends are found. This study suggests a link between the observed increase of summer extreme heat events in the region and the increase of the number of Atlantic depressions. The failure of CMIP6 models to reproduce these events can consequently also reside in an incorrect reproduction of this specific feature of midlatitude atmospheric dynamics.

Plain Language Summary Extreme temperatures events in Western Europe have been rising fast, and current global climate models are not able to reproduce this excess. There are different hypotheses to explain this discrepancy. One is that the large-scale atmospheric dynamics, responsible for the local weather, is not correctly represented by the models: indeed, the frequency and amplitude of some specific weather phenomena have been shown to be insufficiently reproduced, especially in summer. Here, we study one such phenomenon, namely the transient deep depressions, or extratropical cyclones, that travel across the Atlantic basin. A significant large increase of the number of these events is found in summer in the region of the North Atlantic off the western European coast. Depressions in that region are accompanied by high temperatures in continental western Europe. An ensemble of state of the art climate models are also analyzed and none of them is able to correctly reproduce the frequency of deep depressions nor their large trend, which suggests a common origin with the insufficient prediction of western European extreme heat events. Great caution should be used when analyzing climate change predictions in the region, and even more so when studying changes in complex dynamical phenomena.

Key Points:

- Deep depression occurrences have significantly increased over the eastern side, and decreased over the western side of the North Atlantic
- Deep depressions are linked to high surface temperature patterns in western continental Europe but have little impact on the mean warming
- Global Climate Models fail to reproduce the observed trends in deep depressions correctly

Supporting Information:

Supporting Information may be found in the online version of this article.

Correspondence to:

F. D'Andrea,
dandrea@lmd.ipsl.fr

Citation:

D'Andrea, F., Duvel, J.-P., Rivière, G., Vautard, R., Cassou, C., Cattiaux, J., et al. (2024). Summer deep depressions increase over the Eastern North Atlantic. *Geophysical Research Letters*, *51*, e2023GL104435. https://doi.org/10.1029/2023GL104435

Received 7 MAY 2023
Accepted 9 FEB 2024

Author Contributions:

Conceptualization: Fabio D'Andrea, Jean-Philippe Duvel, Gwendal Rivière, Robert Vautard, Christophe Cassou, Julien Cattiaux, Dim Coumou, Tamara Happé, Aglaé Jézéquel, Aurelien Ribes, Pascal Yiou
Data curation: Fabio D'Andrea
Formal analysis: Fabio D'Andrea
Investigation: Fabio D'Andrea
Methodology: Fabio D'Andrea
Resources: Fabio D'Andrea
Software: Fabio D'Andrea
Supervision: Fabio D'Andrea
Validation: Fabio D'Andrea, Jean-Philippe Duvel, Gwendal Rivière, Robert Vautard, Christophe Cassou,

1. Introduction

Climate has been warming quickly in Western Europe. Over mainland France, for instance, mean daily temperatures estimated over the 1950–2022 period, show an increase of more than 1.5°C as a response to climate change (Ribes et al., 2022), and mean daily maximum temperatures in the region have been measured to increase twice to three time as much as the global mean (Vautard et al., 2023). More notably, heatwaves are increasing, as illustrated by several unprecedented events in the last 20 years, with a number of observed record-breaking temperatures exceeding those expected in a stationary climate (Bador et al., 2016). While climate projections show an increase of extreme temperatures in Western Europe with climate change, the amplitude is only captured by very few current climate simulations (Boé et al., 2020; Ribes et al., 2022; van Oldenborgh et al., 2009, 2022).

There is growing evidence that this amplified warming is a result of changes in atmospheric circulation. Using circulation analogs, Vautard et al. (2023) distinguished atmospheric patterns likely to explain such discrepancy,

Julien Cattiaux, Dim Coumou, Tamara Happé, Aglaé Jézéquel, Aurelien Ribes, Pascal Yiou
Visualization: Fabio D'Andrea
Writing – original draft: Fabio D'Andrea
Writing – review & editing: Jean-Philippe Duvel, Gwendal Rivière, Robert Vautard, Christophe Cassou, Julien Cattiaux, Dim Coumou, Tamara Happé, Aglaé Jézéquel, Aurelien Ribes, Pascal Yiou

where large scale zonal pressure gradient systems enhance southerly flow and anticyclonic conditions over the continent. A similar pattern encompassing a low-pressure system (named a *depression* hereafter) over the eastern Atlantic was found by Faranda et al. (2023), still by an analogue approach on historical data, as the pattern with the highest increase in frequency in the region, always linked to extreme temperatures. Southerly advection is not the only mechanism that potentially explains how Atlantic depressions can bring about a warming of continental Europe. On a heatwave case study, Zschenderlein et al. (2019) showed that upper tropospheric ridges on the eastern flank of a depression can prevail over horizontal advection of temperature, via enhanced adiabatic heating by subsidence, or also by diabatic heating at the surface. Indeed, in recent times a number of persistent depressions off the European Atlantic coast have accompanied high or even record breaking temperatures at different locations over the continent. The events of June 2019 and July 2022 made headlines in the mainstream press. Diabatic heating in the storm track upstream of a blocking anticyclone can also bring additional upper-level heat into the block, such as in the Pacific-Northwest American heatwave of 2021 (Schumacher et al., 2022).

Motivated by the above works, we develop a simple objective algorithm to count and characterize deep depressions, and we apply it to the Atlantic/European region in summer. The focus of this paper is to investigate the synoptic aspects of the depressions and their long term evolution in up-to-date reanalyzed and modeled data. Analyzing their precise physical link with heatwaves is deferred to a forthcoming paper. In previous literature, extratropical depressions are comparatively less studied in summer, and never in the context of high temperature events in Europe; a review can be found in Feser et al. (2015). In Section 2, the algorithm is described in detail, as well as the data used. In Section 3, the algorithm is applied to reanalyzed geopotential fields for the whole North Atlantic region and the results are compared to the storm track and baroclinicity. In Section 4, attention is concentrated on the region of the Eastern Atlantic where the strongest evolution of the number of depresssions is found; temperature composites are also shown. In Section 5 an ensemble of global climate models outputs is analyzed with the same methodology. Section 6 is where the results are summarized and discussed with some detail.

2. Data and Methods

Reanalyzed data from ERA5 (Hersbach et al., 2023) are used for the Northern summer months of June July and August (JJA) from 1950 to 2022. Hourly Geopotential fields at 500 hPa (z500) are used with a time step of 24hr hr, at 12 UTC at a grid resolution of 0.25°. Depressions are identified from minima of z500 anomalies; the precise methodology is detailed below. The NCEP reanalysis (Kalnay et al., 1996) is also used in the same manner for comparison, but the main analysis is shown for ERA5.

The region considered covers the North Atlantic and Europe. Long term trends in the number of days with depression occurrence and the long-term dynamical change are analyzed. Successively, a region in the Eastern Atlantic off the Western European coast is singled out, and the composites of temperature maps are computed.

The depression search has also been applied to the output of climate models participating in the Coupled Model Intercomparison Project 6 (CMIP6, Eyring et al., 2016). The list of the models analyzed, with some additional information is found in the Supporting Information S1 (Table S1). The daily z500 output of all models was re-interpolated on the same grid as ERA5, and then the algorithm as described below has been applied.

The precise methodology used is detailed as follows:

1. We consider squares of 15° × 15° in the Euro-Atlantic region with an increment of 1° of latitude and longitude between 65 and 20°N and between 80°W and 20°E.
2. The minimum z500 anomaly with respect to long term mean is found in each square.
3. The minimum is tested for depth (refer to the schematics in Text S1.1 in Supporting Information S1): starting from the gridpoint of the minimum, we consider a segment of $\Delta\lambda = 10$ degrees of longitude or latitude in the four cardinal directions. Along the segment we select the maximum z500 anomaly; if the difference between this maximum and the central minimum exceeds an amplitude $A = 110$ m in all the directions, we retain it as a deep depression (DD).
4. If a given day has a DD selected, it is retained as a DD-day for the central point of the square of 15° × 15° in longitude-latitude.

There are two arbitrary parameters in this algorithm: A and $\Delta\lambda$. The value of $A = 110$ m is chosen according to the distribution of all depths of z500 minima in the region over the Eastern Atlantic described in Section 3 below;

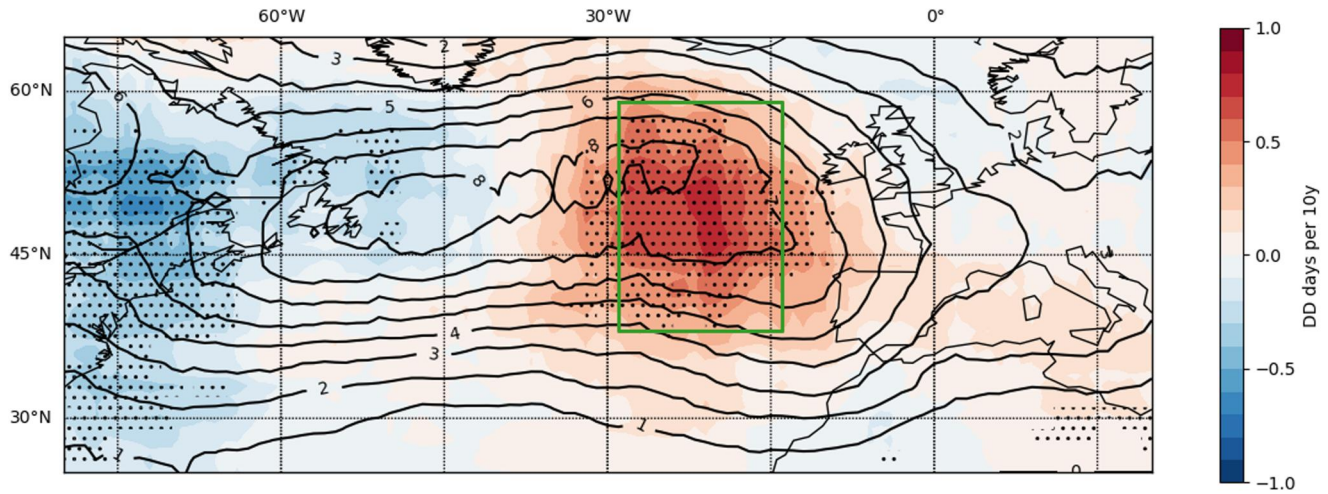

Figure 1. Average number of DD-days per summer (contours) and slope of the linear trend in the number of DD expressed as days per ten years (colors). Hatching indicates regions for which the trend is significant to a Mann-Kendall test with $p < 0.05$. The green rectangle indicates the chosen region for the analysis in Section 4.

110 m corresponds to the 75th centile. The width $\Delta\lambda$ is not a very sensitive parameter. More details on the choice of the parameters and sensitivity to their changes are found in the Text S10 in Supporting Information S1.

3. Trend in Deep Depression Days

The result of the search for deep depressions in the Euro Atlantic region is shown in Figure 1. The average number of DD-days per summer is maximum approximately along the mean location of the summer storm track region (Figure 2a). A positive and statistically significant ($p < 0.05$) trend is found East-Southeast of the maximum. Conversely, a significantly negative linear trend is found west of the domain, along the North American eastern coast.

Climatological studies of extratropical cyclones make use of different metrics, based for example, on relative or potential vorticity, and have methods for tracking trajectories on top of criteria for displacement speed and lifetime, so that a direct comparison with the present work is not straightforward. A comparison of different cyclone tracking methods is found in Raible et al. (2008). They found for summer between 5 and 15 cyclones per square of 1000 km of side and a pattern similar to the solid lines of Figure 1. (see e.g. their Figure 2). The trend shown in Figure 1 is computed on the whole ERA5 period, which means that along the 73 years there is practically a doubling of the number of summer DD-days at the location of the maximum trend and around. The field significance of Figure 1 has also been tested as in Wilks (2016), see Text S9 in Supporting Information S1. In the following, the trends of other physical variables are shown in the region.

The summer stormtrack activity, defined in a classical way as the 2–7 days band pass filtered standard deviation, is shown in Figure 2a for z500. It shows a significant—albeit smaller—linear trend entirely consistent with the evolution in the number of DD-days: negative on the west and positive in the east/southeast. This shift of the summer stormtrack was also observed by Deng et al. (2022) along with the shift in position of the jet that will be discussed below. The decrease of stormtrack activity in the baroclinic region of the American East continental coast is explained by the reduced baroclinicity, measured by use of the Eady growth rate σ as defined in Hoskins and Valdes (1990):

$$\sigma = \alpha f \left| \frac{\partial u}{\partial z} \right| N^{-1},$$

where N is the Brunt-Vaisala frequency. The Eady growth rate is computed for the 850-500 hPa layer; f is the Coriolis parameter, u is the wind speed vector, and α is a factor, estimated to 0.31 by Lindzen and Farrell (1980) from maximum growth rate in baroclinic instability problems.

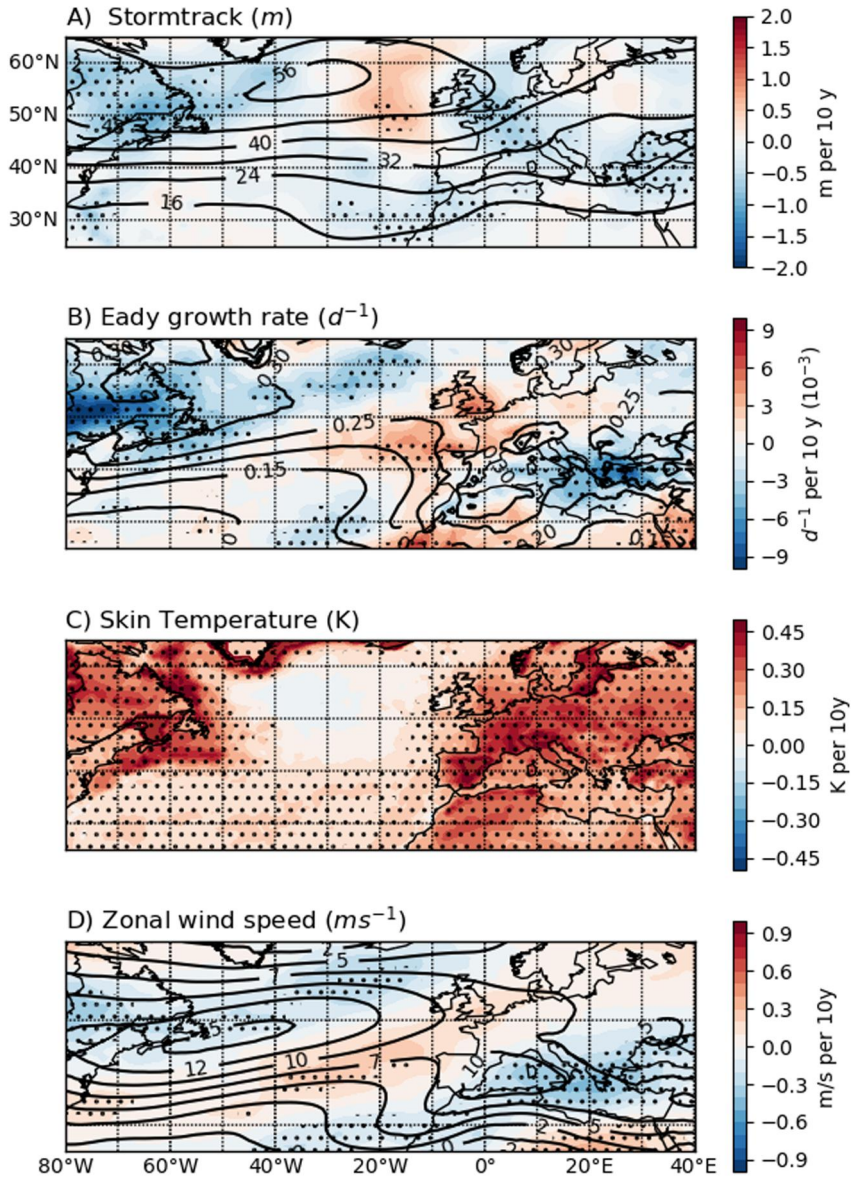

Figure 2. (a) Visualization of the summer storm-track as standard deviation of high-frequency of geopotential height at 500 hPa. Mean field for JJA in the period 1950–2022 in contour. In color the linear trend on JJA yearly mean fields expressed as meters per decade periods. (b) Eady growth rate in the 500–850 hPa layer. As in (a), the black contours are the mean field expressed in days^{-1}, in color is the linear trend in this case expressed as days^{-1} per decade period. (c) Skin temperature: linear trend in Kelvin per 10 years period. (d) Linear trend of the 500 hPa zonal wind in meters per second per decade. The mean field for the whole period is in contours. In all panels the areas of trend significant to a Mann-Kendall test with $p < 0.05$ are stippled.

The Eady growth rate is shown in Figure 2b. It strongly decreases over Labrador and along the American continental coast. This is explained by the strong increase in surface temperature, visible on Figure 2c, that creates a diminished meridional temperature gradient at higher levels, reducing the wind shear. This is better visible in the maps of temperature trends at higher levels, that are shown in the Figure S6 in Supporting Information S1. Note that the change in σ is largely dominated everywhere by the change in wind shear, and not by change in the static stability (not shown). On the other side of the basin, northwest of the Iberian peninsula, an increase in baroclinicity accompanies the increase in stormtrack activity. This is consistent with the enhanced meridional temperature gradient and the accelerated zonal wind that increases the vertical wind shear: the wind (Figure 2d) decreases on the west north Atlantic coast, consistently with the reduced stormtrack, while it is shifted southwards

on the east of the basin. Note that the southward shift of the jet stream at that location was already documented for the more recent period starting in 1979 by Simmons (2022). The same analysis as in Figure 2 has been repeated with no substantial differences for the period 1979–2022 and for the upper layer 250–500 hPa. See Figures S4 and S5 in Supporting Information S1.

4. Eastern Atlantic Depression Increase

In this section, a region straddling the area of positive trend seen in Figure 1 is selected, shown as a green rectangle, and the deep depressions (DDs) occurring inside this region are counted. The relation of these events to Western European temperature is also computed. The region spans longitudes 14°W to 29°W and latitudes 38°N to 59°N. As before, this region is scanned by partially overlapping squares of 15° in longitude-latitude. The difference here is that when a deep depression is found in a given day for at least one of the squares, the day is retained as a deep depression day (DD-day) for the whole region; this allows harnessing more events.

A total of 724 DD-days were found for the whole period in the region, which corresponds to around 10 days per summer on average—summer counting 92 days—although large year to year variations are present, as will be shown below. There is no seasonal cycle, the number of DD-days is not significantly different in either of the three summer months (not shown).

A composite map of the DD-days anomalies is shown for illustration in the Figure S7 in Supporting Information S1. The synoptic structures of the selected depressions can be either cut off from the core of the westerly flow, or can be large troughs embedded in the jet. In Figures S8 and S9 in Supporting Information S1 there are examples of the two: the cut off lows in June 2019 that were associated with a strong heatwave, and the deep troughs of August 2012. A simple criterion can be added to the DD definition in order to distinguish between the two kinds, checking the latitudinal position of the minimum z500 with respect to the position of the jet. This analysis (not shown) gives 17% of DD-days due to cut-off lows; both kinds show a significant increasing trend and only fine differences with respect to what shown in Figure 3, so for the moment both will be considered indifferently. For a climatology and dynamics of cut-off lows see Nieto et al. (2005).

The bar plot in Figure 3a shows the count of DD-days between 1950 and 2022 in ERA5. A positive trend and a large year-to-year variability are visible. The linear trend is highly significant to a Mann-Kendall test with a p-value $p = 2 \cdot 10^{-4}$ and almost doubles the number of DD-days across the 73 years period, consistently with Figure 1. The average number of DD-days per summer is 7.6 in the period 1950–1974 and 12 in the period 1998–2022. The linear trend computed from the NCEP reanalysis is also shown by the dashed line. The two reanalyses have the same linear trend, while NCEP counts approximately one DD-day less per summer; a more detailed comparison can be found in Text S2 in Supporting Information S1.

We construct the composite maps of 2-m temperature at 14:00 UTC (2mT) by averaging 2mT anomaly fields for all 724 DD-days; to reduce the impact of global warming, the 2mT time series has been linearly detrended before computing the composite. This avoids putting more weights on the end of the period, when temperatures are higher and DD-days more frequent. The resulting pattern is in Figure 3b, where practically all areas of continental Europe are statistically significant to a *t*-test with $p < 0.05$. It can be seen that DDs in the region are accompanied by high temperatures in central-western Europe. The pattern in Figure 3b resembles closely the pattern of excess extreme heating of Vautard et al. (2023, Figure 1a), as well as the typical anomalous temperature pattern during West-European heatwaves (Stefanon et al., 2012, Figure 2).

This composite pattern hints at a relevance of the DD to extreme temperatures in western Europe, but a quantitative analysis of this relevance is deferred to a future paper. Here, we limit ourselves to estimating the effect of the increase of DD-days on the mean 2mT. This can be done by comparing the trend of 2mT during the non-DD-days to the total trend: the difference is the contribution of the increase of DD-days. For the area delimited by the green rectangle in Figure 3b, the difference between these trends is 0.03 K/10y, which brings about a total excess mean heating of 0.2 K along the ERA5 73 years period. Given that the total increase of 2mT at 14:00 in the same period is 3.4 K, we can say that the contribution, though statistically significant, is small. See Figures S10 and S11 in Supporting Information S1.

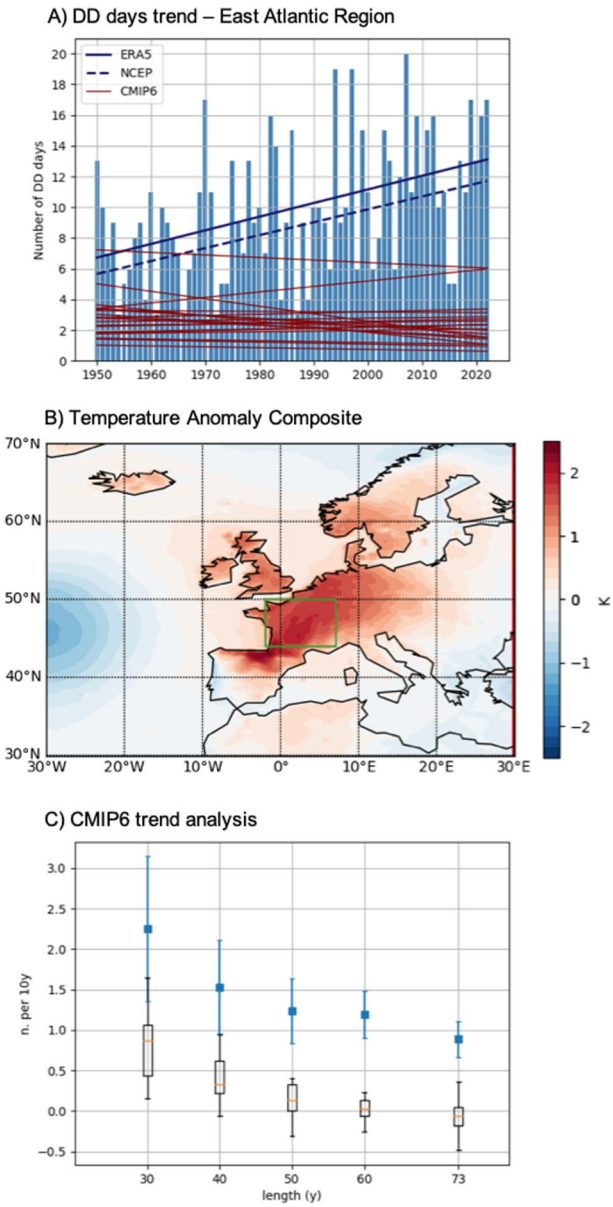

Figure 3. (a) Bars: number of DD-days per summer in ERA5 in the Eastern Atlantic region shown in green in Figure 1; linear interpolation in dark blue. Dark red lines are the result of the same analysis on a sample of CMIP6 models outputs, only the linear interpolation is shown, dark blue dashed is the same for the NCEP reanalysis; see text Section 5. (b) Composite map of detrended 2 m temperature anomaly at 14:00 UTC for all DD-days. The green box is the region for which the DD-days contribution to the mean temperature is computed (see text). (c) Maximum value of the linear trend for different period lengths. Blue: ERA5 with 95% confidence interval. Box-whiskers plot: CMIP6 models. Trends are expressed as the number of DD-days per decade.

5. Deep Depressions in CMIP6 Models

A sample of 20 historical integrations from 20 different models has been selected, and geopotential height daily output at 500 hPa has been analyzed. The same procedure as in Section 4 has been applied to the model outputs, their results are represented superposed to those of ERA5 in Figure 3a; the yearly bars are not plotted for the models, only the estimated linear trend is displayed as the thin dark red lines. In general models have a lower mean count of DD-days compared to ERA5, and only one simulation yields a positive trend, but it is not significant.

In Figure 3c the trends in the number of depressions is explored for shorter durations of time. The maximum positive trend found for the durations of 30–73 years—included in the 1950–2022 period—are shown in the figure, as a function of the trend length. The results for ERA5 are compared to the distribution of the CMIP6 models trends. CMIP6 models do not manage to reproduce the positive trends detected in the reanalyses, and their difference with ERA5 seems to increase with the length considered.

It is not surprising that the number of DD-days is underestimated in CMIP6 models. Harvey et al. (2020) documented a weakening and northward shift of the summertime stormtrack in the subsequent generations of CMIP models including the 6th. A weakening of blocking frequency is equally found by Davini and D'Andrea (2020). Different reasons have been brought forward to explain this decreasing variability; they include low spatial resolution (Zappa et al., 2013), orography (Berckmans et al., 2013), or biases in surface temperature (Keeley et al., 2012).

While it would be useful to analyze each individual model in order to identify the dynamical origin of its own reduced variability, a quick test can be carried out reducing the parameter A, that is, the depth of the z500 minima, in order to account for the reduced variability and increase the mean number of DD-days found. The equivalent of Figures 3a and 3c are found in the Figures S12 and S13 in Supporting Information S1, for $A = 70$ m. With this choice, the mean number of DD-days in the models is approximately equivalent to ERA5, but still no model matches the increasing trend, with the exception of MPI-ESM1-2-HR that has a significant positive trend with $p = 0.04$. The individual behavior of each model is also displayed in Figure S14. In Figure S15 in Supporting Information S1 the same as Figure 1 is represented for each model individually, still in this "boosted" configuration using $A = 70$ m. Some models have marginally significant trends, most of the time negative in different regions. IPSL-CM6A-LR reproduces the decrease of DD-days in the western Atlantic region but not the increase in the East. The only—but little significant - models that have a pattern of DD trends resembling ERA5 are ACCESS-CM2 and MPI-ESM1-2-HR.

6. Summary and Discussion

A simple algorithm for counting events of deep depression has been applied to the North Atlantic/European region. The number of Deep Depressions (DD) days during summer has almost doubled in the eastern Atlantic region since 1950. Such a trend has not been shown in preceding studies: there is some consensus of an increase of storminess at high latitudes in the eastern north Atlantic, and of a decrease south of it, off the British Isles, although not specifically in summer (see Freser et al., 2015 and references therein). But a direct comparison with the present work is not straightforward, for here we seek depressions at a higher level in the troposphere. The same algorithm applied to ERA5 data has also been applied to a sample of CMIP6 model outputs, and no trend is found, in agreement with recent storminess analysis like Priestley and Catto (2022).

DD-days are accompanied by higher temperatures in western and central Europe, with a pattern that has been linked to temperature extremes in previous literature. While the effect of the increase of Atlantic depressions is limited on the mean summer 2mT in the western European region, this study suggests that it could be relevant for the increase of heatwaves, via southerly temperature advection or other mechanisms. The failure of CMIP6 models to reproduce this increase can consequently be linked to the incorrect reproduction of these dynamical features or to a large-scale perturbation at the origin of both phenomena. This is in good agreement with studies like Vautard et al. (2023) and Faranda et al. (2023).

Despite some consistent dynamical context of the increase of DDs given in this paper, an explanation of the reasons for the phenomenon remains insufficient. It is moreover unclear whether the trend comes from natural variability of the midlatitude flow or whether it is due to some large-scale forcing, of natural or human-induced origin. Going back to Figure 1 of this paper, while it is reasonable to think that the surface warming on the American continent decreases the jetstream and the stormtrack in the western Atlantic, it is less clear why there is an increase of activity in the eastern side. The increase in baroclinicity there is due to an increase of the vertical shear of the wind and not to a change in vertical stability (not shown). The increased vertical shear is associated with a southeastward shift of the jet. The causal relation of the increased wind speed with the presence of increased cyclones in the area remains however undecided.

Other aspects of the summer midlatitude circulation are undergoing rapid modifications in reanalyzed data. A strong positive trend has been observed for instance in the number of Greenland blocking events. This increase has been suggested as a cause for Greenland continental temperature increase and ice depletion (Hörhold et al., 2023 and references therein), but a dynamical understanding of this phenomenon is still absent. Furthermore, Dong et al. (2013) also found a southward shift of the Atlantic stormtrack activity and changes of baroclinicity similar to Figure 2b, and linked those to the Greenland blocking increase. In addition, it is notable that CMIP6 models also fail in reproducing the Greenland blocking increase (Davini & D'Andrea, 2020).

There have been advances in explaining the dynamics of the increase of heatwaves (see e.g. Hoffman et al., 2021) and other kinds of persistent anomalies causing hydroclimatic extrema, but it is fair to say that a full picture is still not available. Arctic Amplification has been proposed as a possible large-scale forcing for weakening of summer storm tracks (Coumou et al., 2015), but aerosol forcings could also play a role (Dong et al., 2022). Different mechanisms have been proposed in driving quasi-stationary Rossby waves, including waveguide-effects, (Kornhuber et al., 2017), soil-moisture depletion (Teng & Branstator, 2019) and zonally asymmetric thermal forcing (Moon et al., 2022). Whether or not such quasi-stationary waves are increasing is debated but there are indications for an increase in wave number 5 (Teng et al., 2022) and associated zonal-mean double-jet states (Rousi et al., 2022).

A number of ideas originating from this work deserve further research. First of all, the relevance of the DD increase on extreme temperature has to be quantified. In fact, recent summer heatwaves (such as in 2022 or 2019) have been accompanied by persistent cut-off low patterns. This analysis is deferred to a forthcoming paper. DDs or cut-off lows are not the only patterns creating heatwaves, of course: persistent high-pressure systems over the western European regions are also very common. It will be interesting to study in detail the interaction between DDs and high-pressure systems over continental Europe. As discussed in the introduction, DDs can create high-pressure systems at mid troposphere by the increase of temperature in the atmospheric column, and that could actually cause or reinforce a blocking. A high pressure over continental Europe would have a local warming effect but also slow down the low-pressure systems themselves, in the eastern Atlantic region. The analysis presented here does not allow the detection of a significant increase with time of the duration of the DD events; however, it cannot be excluded that the increase of temperature in western Europe could be the cause of the increase of DD over the eastern Atlantic, rather than the effect. As highlighted by Drouard and Woollings (2018) DD can be anticipated by the blocking anticyclone. No long-term trend in atmospheric blocking occurrence is found over western Europe, but an increasing trend in z500 is indeed documented, see for example, Simmons (2022). Dedicated climate model experiments might be used to disentangle this causal relation. In any case, it is notable that the very fact that CMIP6 models do not reproduce the trend of DD-days nor the excess heating of western Europe is an additional hint of the link between the two phenomena. A more refined analysis on the CMIP6 models that do (like MPI-ESM1-2-HR) or do not reproduce the trend could also give information on the causal relation between high-pressure over Europe and DDs.

Whether it is internal or forced variability, it remains clear that CMIP6 models appear to be unable to correctly reproduce the complex dynamical changes happening in the northern extratropical summer, which is likely part of the explanation of the insufficient prediction of increase in western European extreme temperatures. Great caution should be consequently used when analyzing climate change predictions in the region, and even more so when studying changes in complex dynamical phenomena.

Data Availability Statement

All data used is open and publicly available: ERA5 data is available at Hersbach et al. (2023). NCEP-NCAR Reanalysis data is available at Kalnay et al. (1996). CMIP6 data are available from any node of the Earth System Grid Federation (ESGF), see Cinquini et al. (2014). We acknowledge the use of the open source scientific environment spyder: P. Raybaut (2009).

Acknowledgments
Two anonymous reviewers largely contributed to improving the manuscript. FDA thanks Paolo Davini for advice and discussion. RV, DC, DF, TH, and PY acknowledge funding from the European Union's H2020 program grant agreement 101003469 (XAIDA).

References

Bador, M., Terray, L., & Boé, J. (2016). Emergence of human influence on summer record-breaking temperatures over Europe. *Geophysical Research Letters*, *43*(1), 404–412. https://doi.org/10.1002/2015GL066560

Berckmans, J., Woollings, T., Demory, M.-E., Vidale, P.-L., & Roberts, M. (2013). Atmospheric blocking in a high resolution climate model: Influences of mean state, orography and eddy forcing. *Atmospheric Science Letters*, *14*(1), 34–40. https://doi.org/10.1002/asl2.412

Boé, J., Terray, L., Moine, M. P., Valcke, S., Bellucci, A., Drijfhout, S., et al. (2020). Past long-term summer warming over western Europe in new generation climate models: Role of large-scale atmospheric circulation. *Environmental Research Letters*, *15*(8), 084038. https://doi.org/10.1088/1748-9326/ab8a89

Cinquini, L., Crichton, D., Mattmann, C., Harney, J., Shipman, G., Wang, F., et al. (2014). The Earth System Grid Federation: An open infrastructure for access to distributed geospatial data [Dataset]. Future Generation Computer Systems, *36*, 400–417. https://doi.org/10.1016/j.future.2013.07.002

Coumou, D., Lehmann, J., & Beckmann, J. (2015). The weakening summer circulation in the Northern Hemisphere mid-latitudes. *Science*, *348*(6232), 324–327. https://doi.org/10.1126/science.1261768

Davini, P., & D'Andrea, F. (2020). From CMIP3 to CMIP6: Northern Hemisphere atmospheric blocking simulation in present and future climate. *Journal of Climate*, *33*(23), 10021–10038. https://doi.org/10.1175/jcli-d-19-0862.1

Deng, K.-Q., Azorin-Molina, C., Yang, S., Hu, C.-D., Zhang, G.-F., Minola, L., et al. (2022). Shifting of summertime weather extremes in Western Europe during 2012–2020. *Advances in Climate Change Research*, *13*(2), 218–227. https://doi.org/10.1016/j.accre.2022.01.008

Dong, B., Sutton, R. T., Shaffrey, L., & Harvey, B. (2022). Recent decadal weakening of the summer Eurasian westerly jet attributable to anthropogenic aerosol emissions. *Nature Communications*, *13*(1), 1148. https://doi.org/10.1038/s41467-022-28816-5

Dong, B., Sutton, R. T., Woollings, T., & Hodges, K. (2013). Variability of the North Atlantic summer storm track: Mechanisms and impacts on European climate. *Environmental Research Letters*, *8*(9), 034037. https://doi.org/10.1088/1748-9326/8/3/034037

Drouard, M., & Woollings, T. (2018). Contrasting mechanisms of summer blocking over western Eurasia. *Geophysical Research Letters*, *45*(21), 12040–12048. https://doi.org/10.1029/2018GL079894

Eyring, V., Bony, S., Meehl, G. A., Senior, C. A., Stevens, B., Stouffer, R. J., & Taylor, K. E. (2016). Overview of the Coupled Model Intercomparison Project phase 6 (CMIP6) experimental design and organization. *Geoscientific Model Development*, *9*(5), 1937–1958. https://doi.org/10.5194/gmd-9-1937-2016

Faranda, D., Messori, G., Jezequel, A., Vrac, M., & Yiou, P. (2023). Atmospheric circulation compounds anthropogenic warming and impacts of climate extremes in Europe. *Proceedings of the National Academy of Sciences*, *120*(13), e2214525120. https://doi.org/10.1073/pnas.2214525120

Feser, F., Barcikowska, M., Krueger, O., Schenk, F., Weisse, R., & Xia, L. (2015). Storminess over the North Atlantic and northwestern Europe—A review. *Quarterly Journal of the Royal Meteorological Society*, *141*(687), 350–382. https://doi-org.insu.bib.cnrs.fr/10.1002/qj.2364

Harvey, B. J., Cook, P., Shaffrey, L. C., & Schiemann, R. (2020). The response of the Northern Hemisphere storm tracks and jet streams to climate change in the CMIP3, CMIP5, and CMIP6 climate models. *Journal of Geophysical Research: Atmospheres*, *125*(23), e2020JD032701. https://doi.org/10.1029/2020JD032701

Hersbach, H., Bell, B., Berrisford, P., Biavati, G., Horányi, A., Muñoz Sabater, J., et al. (2023). ERA5 hourly data on pressure levels from 1940 to present [Dataset]. Copernicus Climate Change Service (C3S) Climate Data Store (CDS). https://doi.org/10.24381/cds.bd0915c6

Hoffmann, P., Lehmann, J., Bijan, H., & Hattermann, F. F. (2021). Atmosphere similarity patterns in boreal summer show an increase of persistent weather conditions connected to hydro-climatic risks. *Nature Scientific Reports*, *11*(1), 22893. https://doi.org/10.1038/s41598-021-01808-z

Hörhold, M., Münch, T., Weißbach, S., Kipfstuhl, S., Freitag, J., Sasgen, I., et al. (2023). Modern temperatures in central–north Greenland warmest in past millennium. *Nature*, *613*(7944), 503–507. https://doi.org/10.1038/s41586-022-05517-z

Hoskins, B. J., & Valdes, P. J. (1990). On the existence of storm-tracks. *Journal of the Atmospheric Sciences*, *47*(15), 1854–1864. https://doi.org/10.1175/1520-0469(1990)047<1854:oteost>2.0.co;2

Kalnay, E., Kanamitsu, M., Kistler, R., Collins, W., Deaven, D., Gandin, L., et al. (1996). The NCEP/NCAR 40-year reanalysis project [Dataset]. Bulletin America Meteorology Social, *77*, 437–470. https://doi.org/10.1175/1520-0477(1996)077<0437:tnyrp>2.0.co;2

Keeley, S., Sutton, R., & Shaffrey, L. (2012). The impact of North Atlantic Sea surface temperature errors on the simulation of North Atlantic European region climate. *Quarterly Journal of the Royal Meteorological Society*, *138*(668), 1774–1783. https://doi.org/10.1002/qj.1912

Kornhuber, K., Petoukhov, V., Karoly, D., Petri, S., Rahmstorf, S., & Coumou, D. (2017). Summertime planetary wave resonance in the Northern and Southern Hemispheres. *Journal of Climate*, *30*(16), 6133–6150. https://doi.org/10.1175/jcli-d-16-0703.1

Lindzen, R. S., & Farrell, B. A. (1980). Simple approximate result for the maximum growth rate of baroclinic instabilities. *Journal of the Atmospheric Sciences*, *37*(7), 1648–1654. https://doi.org/10.1175/1520-0469(1980)037<1648:asarft>2.0.co;2

Moon, W., Kim, B.-M., Yang, G.-H., & Wettlaufer, J. S. (2022). Wavier jet streams driven by zonally asymmetric surface thermal forcing. *Proceedings of the National Academy of Sciences of the United States of America*, *119*(38), e2200890119. https://doi.org/10.1073/pnas.2200890119

Nieto, R., Gimeno, L., de la Torre, L., Ribera, P., Gallego, D., García-Herrera, R., et al. (2005). Climatological features of cutoff low systems in the northern hemisphere. *Journal of Climate*, *18*(16), 3085–3103. https://doi.org/10.1175/JCLI3386.1

Priestley, M. D. K., & Catto, J. L. (2022). Future changes in the extratropical storm tracks and cyclone intensity, wind speed, and structure. *Weather Clim. Dynam.*, *3*(1), 337–360. https://doi.org/10.5194/wcd-3-337-2022

Raible, C. C., Della-Marta, P. M., Schwierz, C., Wernli, H., & Blender, R. (2008). Northern Hemisphere extratropical cyclones: A comparison of detection and tracking methods and different reanalyses. *Monthly Weather Review*, *136*(3), 880–897. https://doi.org/10.1175/2007MWR2143.1

Raybaut, P. (2009). Spyder-documentation [Software]. Spyder. Available Online at: Pythonhosted.Org https://www.spyder-ide.org/

Ribes, A., Boé, J., Qasmi, S., Dubuisson, B., Douville, H., & Terray, L. (2022). An updated assessment of past and future warming over France based on a regional observational constraint. *Earth System Dynamics Discussions*, *13*(4), 1–29. https://doi.org/10.5194/esd-13-1397-2022

Rousi, E., Kornhuber, K., Beobide-Arsuaga, G., Luo, F., & Coumou, D. (2022). Accelerated western European heatwave trends linked to more-persistent double jets over Eurasia. *Nature Communications*, *13*(1), 3851. https://doi.org/10.1038/s41467-022-31432-y

Schumacher, D. L., Hauser, M., & Seneviratne, S. I. (2022). Drivers and mechanisms of the 2021 Pacific northwest heatwave. *Earth's Future*, *10*(12), e2022EF002967. https://doi.org/10.1029/2022EF002967

Simmons, A. J. (2022). Trends in the tropospheric general circulation from 1979 to 2022. *Weather and Climate Dynamics*, *3*, 777–809. https://doi.org/10.5194/wcd-3-777-2022

Stefanon, M., D'Andrea, F., & Drobinski, P. (2012). Heatwave classification over Europe and the Mediterranean region. *Environmental Research Letters*, *7*(1), 014023. https://doi.org/10.1088/1748-9326/7/1/014023

Teng, H., & Branstator, G. (2019). Amplification of waveguide teleconnections in the boreal summer. *Current Climate Change Reports*, *5*(4), 421–432. https://doi.org/10.1007/s40641-019-00150-x

Teng, H., Leung, R., Branstator, G., Lu, J., & Ding, Q. (2022). Warming pattern over the Northern Hemisphere midlatitudes in boreal summer 1979–2020. *Journal of Climate*, *35*(11), 3479–3494. https://doi.org/10.1175/JCLI-D-21-0437.1

van Oldenborgh, G. J., Drijfhout, S., van Ulden, A., Haarsma, R., Sterl, A., Severijns, C., et al. (2009). Western Europe is warming much faster than expected. *Climate of the Past*, *5*, 1–12. https://doi.org/10.5194/cp-5-1-2009

Van Oldenborgh, G. J., Wehner, M. F., Vautard, R., Otto, F. E. L., Seneviratne, S. I., Stott, P. A., et al. (2022). Attributing and projecting heatwaves is hard: We can do better. *Earth's Future*, *10*(6), e2021EF002271. https://doi.org/10.1029/2021EF002271

Vautard, R., Cattiaux, J., Happé, T., Singh, J., Bonnet, R., Cassou, C., et al. (2023). Heat extremes in Western Europe are increasing faster than simulated due to missed atmospheric circulation trends. *Nature Communications*, *14*(1), 6803. https://doi.org/10.1038/s41467-023-42143-3

Wilks, D. S. (2016). "The stippling shows statistically significant grid points": How research results are routinely overstated and overinterpreted, and what to do about it. *Bulletin America Meteorology Social*, *97*(12), 2263–2273. https://doi.org/10.1175/BAMS-D-15-00267.1

Zappa, G., Shaffrey, L. C., & Hodges, K. I. (2013). The ability of CMIP5 models to simulate North Atlantic extratropical cyclones. *Journal of Climate*, *26*(15), 5379–5396. https://doi.org/10.1175/JCLI-D-12-00501.1

Zschenderlein, P., Fink, A. H., Pfahl, S., & Wernli, H. (2019). Processes determining heat waves across different European climates. *Quarterly Journal of the Royal Meteorological Society*, *145*(724), 2973–2989. https://doi.org/10.1002/qj.3599